Discover Nano

Research

Citric acid based ($CQDs/TiO_2$) nanocomposites against SARS-COV-2: theoretical, photocatalytic and computational studies

Joina Gunjan Singh[1] · Ankit Kumar Singh[1,2] · Nurul Hidayah Mohamad Idris[3] · Nattasa Kitchawengkul[4] · Purim Jarujamrus[4] · Hooi Ling Lee[3] · Maria Grishina[5] · Nadezhda Palko[5] · Prateek Pathak[1,6] · Amita Verma[1]

Received: 21 July 2024 / Accepted: 24 September 2024
Published online: 02 December 2024

Abstract
In the last decade, carbon quantum dots (CQDs), a novel class of carbon-based nanomaterials, have received increasing attention due to their distinct properties. Carbon Quantum Dots/Titanium Dioxide ($CQDs/TiO_2$) Nanocomposites were reported as potent compounds against SARS-COV-2. In this manuscript, citric acid is the carbon precursor used to synthesize carbon quantum dots (CQDs). Using a green approach, the synthesized CQD fabricates the Carbon Quantum Dots/Titanium Dioxide (CQDs/TiO2) Nanocomposites. Synthesized composites were characterized by using a UV–visible spectrophotometer, Fourier-transformed infrared (FTIR) spectrometry, X-ray diffractometry (XRD), and Scanning electron microscopy with energy dispersive X-ray analysis (SEM–EDX). Methylene blue was used to check the Photocatalytic activity of synthesized ($CQDs/TiO_2$) nanocomposites of different concentrations. Computational modeling of agglomerates of CQD and TiO2 nanoparticles with the formula TiO_2…….. $Ti_{253}O_{506}$ demonstrated two stages of the nanocomposite formation, including the formation of agglomerates with the neutral and salt-like structures with the total gain in the Gibbs free energy − 38.397 kcal/mole. In silico, Molecular docking studies of citric acid were evaluated against SARS-COV-2 protein to understand their mechanism and key amino acid interactions along with standard drug remdesivir. The photocatalytic activity of $CQDs/TiO_2$ showed extremely promising results. Based on this study, the proposed mechanism of action of these compounds is reported. A detailed investigation of $CQDs/TiO_2$ against SARS-CoV-2 is needed, which is another part of the research in our next manuscript.

Keywords Citric acid · $CQDs/TiO_2$ · Nanocomposites · SARS-COV-2 · Photocatalytic

Abbreviations

CQDs	Carbon quantum dots
$CQDs/TiO_2$	Carbon Quantum Dots/Titanium Dioxide
FTIR	Fourier Transformed Infrared

Joina Gunjan Singh and Ankit Kumar Singh have contributed equally to this manuscript.

✉ Amita Verma, amitaverma.dr@gmail.com | [1]Bioorganic and Medicinal Chemistry Research Laboratory, Department of Pharmaceutical Sciences, Sam Higginbottom University of Agriculture, Technology & Sciences, Prayagraj 211007, India. [2]Department of Pharmaceutical Sciences and Natural Products, Central University of Punjab, Ghudda, Bathinda 151401, India. [3]Nanomaterials Research Group, School of Chemical Sciences, Universiti Sains Malaysia (USM), 11800 Gelugor, Penang, Malaysia. [4]Department of Chemistry and Center of Excellence for Innovation in Chemistry, Faculty of Science, Ubon Ratchathani University, Ubon Ratchathani 34190, Thailand. [5]Laboratory of Computational Modelling of Drugs, Named After Potemkin V.A. of the South Ural State University, Prospect Lenina-76, Chelyabinsk 454080, Russia. [6]Laboratory of Drug Discovery, Department of Pharmaceutical Analysis, Quality Assurance and Pharmaceutical Chemistry, School of Pharmacy, GITAM (Deemed to Be University), Hyderabad Campus, Hyderabad 502239, India.

SEM	Scanning Electron Microscope
MB	Methylene blue
PDT	Photodynamic therapy
PSs	Photosensitizers
XRD	X-ray Diffraction

1 Introduction

Carbon quantum dots (CQDs) are a novel class of nanomaterials that have recently received a lot of attention due to their unique properties such as small size, high surface area, photoluminescence, chemical stability, tunable optoelectronic property, low toxicity, excellent biocompatibility, superior photostability, and ease of synthesis and functionalization. Other distinguishing characteristics of CQDs include excellent electronic properties (electron donors and acceptors), up-converting and size-dependent photoluminescence, chemical inertness, and photostability. They are carbon nanostructures smaller than 10 nm with fluorescent properties [1–4]. They are highly appealing for nanomedical applications because animals have no visible signs of toxicity. It has recently been demonstrated that CQDs are appropriate scaffolds to interfere with the entry of viruses into cells [5]. These CQDs were accidentally discovered while purifying single-walled carbon nanotubes prepared using arc-charged methods. CQDs are currently being widely studied in the field of photocatalysis. Tang et al. synthesized CQDs-TiO_2 composites using titanyl sulfate as the titanium source and graphite rods electrolyzed in a hydrothermal reaction [6]. There are two synthetic methods for CQDs: "top-down" and "bottom-up." The "top-down" approach is typically a physical or chemical method for producing small-sized CQDs peeling from large-scale carbon. The "bottom-up" method always begins with small molecule carbon sources such as critic acid. CQDs are produced using methods involving hydrothermal/solve thermal treatment, ultrasonic treatment, microwave irradiation, laser ablation, and electrochemical carbonization [7, 8]. CQDs-based biomacromolecule detection has demonstrated excellent performance and feasibility in point-of-care testing for viruses [7]. Photodynamic therapy (PDT) is a novel way to kill viruses. PDT was used clinically against viruses for the first time since the 1970s [25]. A suggestion about the potential efficiency of a PDT against SARS-CoV-2 was made relatively recently, and brief results on the use of PDT in humans were also published [9]. The principle of PDT involves the activation of a photosensitizer, absorb visible light to primarily form the excited singlet state, which eventually transforms into the excited triplet state, which responds to light and leads to photochemical reactions with oxygen to produce reactive oxygen species (ROS) that kill microbes (Fig. 1) [10]. Many photosensitizers (PSs) made from various chemical compounds are used in PDT, including methylene blue (MB), which is classified as a medicinal drug in the Russian Federation. MB is a phenothiazine compound with photosensitizing properties [11].

In this study, citric acid is the carbon precursor used to synthesize carbon quantum dots (CQDs). Using a green approach, the synthesized CQD fabricates the Carbon Quantum Dots/Titanium Dioxide (CQDs/TiO2) Nanocomposites. Synthesized compounds were characterized by using a UV–visible spectrophotometer, Fourier-transformed infrared (FTIR) spectrometry, X-ray diffractometry (XRD), and Scanning electron microscopy with energy dispersive X-ray analysis (SEM–EDX). MB was used to check the photocatalytic activity of synthesized (CQDs/TiO_2) nanocomposites. Computational modeling and in silico Molecular docking studies of synthesized compounds were evaluated against SARS-COV-2 protein to understand their mechanism in SARS-COV-2 protein interaction.

2 Methodology

2.1 General procedure of synthesis

All the reagents and solvents were purchased from Sigma-Aldrich, Spectrochem Pvt. Ltd, TCI India Chemicals pvt. Ltd and was used without further purification. 1.20 g of citric acid was weighed and transferred to a beaker; 50 mL of distilled water was added. The solution was kept under ultrasonication continuously for 20 min. After 20 min of continuous stirring, the solution was transferred to the Teflon autoclave. Then, it was placed in an oven at 180 °C for 5 h. After 5 h in the oven, it was removed and cooled completely. The solution inside the Teflon autoclave was found to be reduced to 60%, and there was also a color change. The confirmation of prepared citric acid CQDs was done by UV lamp at 365 nm, which shows blue color fluorescence (Fig. 2). Purification and separation of CQDs were done by dialysis in a 1 kDa dialysis tube

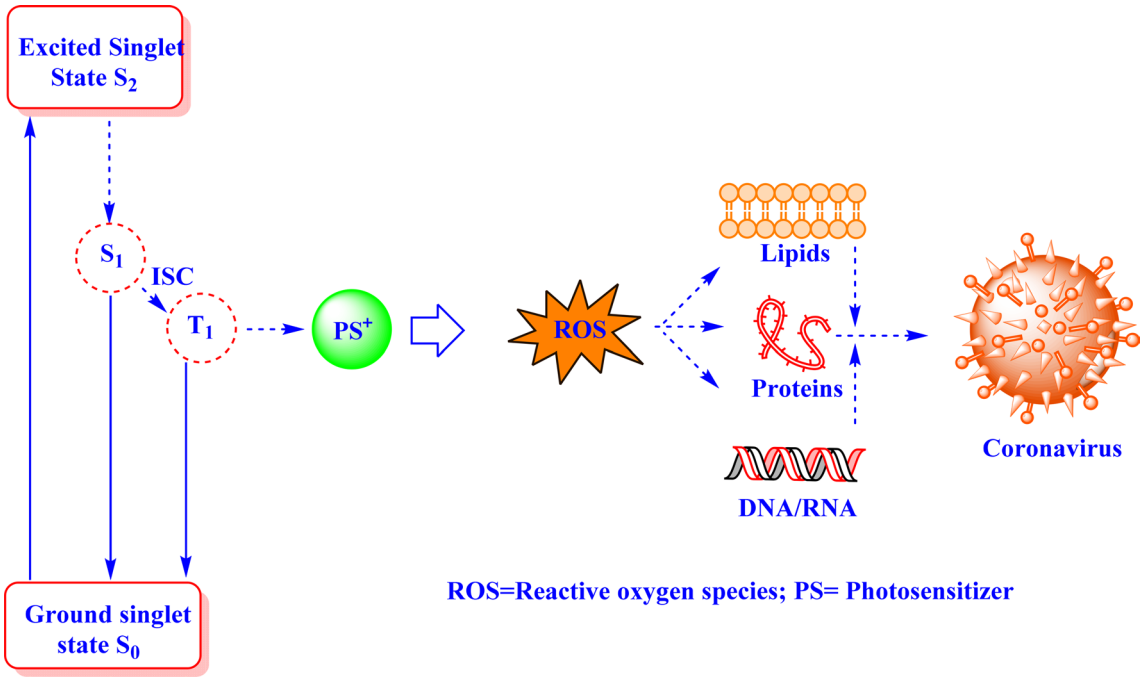

Fig. 1 Mechanism of PDT in virus killing

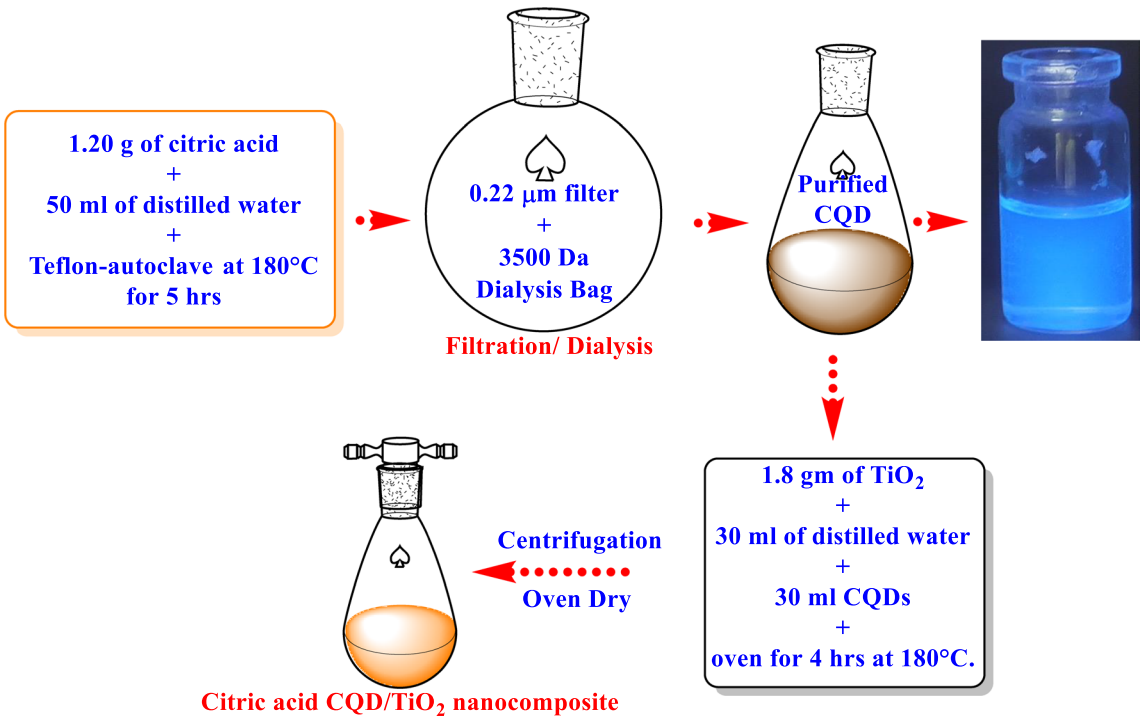

Fig. 2 Synthesis of Nanocomposites of citric acid carbon quantum dots with TiO_2 nanoparticles

and centrifuged at 8400 rpm for 15 min to remove unreacted starting materials. Finally, the brown clear solution was obtained, stored at 4 °C in the refrigerator, and protected from light for future use.

2.1.1 Synthesis of nanocomposites of citric acid carbon quantum dots with TiO_2 nanoparticles

A beaker contained 1.8 g of Titanium dioxide and 30 mL of distilled water. The suspension was then stirred continuously for 60 min. After 60 min of stirring, 30 mL of prepared CQDs were added to the beaker and stirred continuously for 5 to 10 min. The mixture was then transferred to a Teflon autoclave and placed in an oven at 180 °C for four hours. After 4 h, the Teflon autoclave was removed and completely cooled down. The mixture is reduced, and a precipitate is formed. The mixture is then centrifuged to remove unwanted material by washing it three times with distilled water and ethanol at 15,000 rpm for 10 to 15 min. Then, it is dried and stored (Fig. 2). Purification and separation were done by dialysis in a 1 kDa dialysis tube and centrifuged at 8400 rpm for 15 min. Finally, the cream solution was stored at 4 °C in the refrigerator and was subjected to characterization [8, 12, 13].

2.2 Characterization

The structural characterization and morphology of the obtained CQDs and CQDs/TiO_2 nanocomposite samples were investigated using the following methods.

2.2.1 UV–vis spectroscopy

UV–visible spectrophotometric analysis was performed on a synthesized CQDs/TiO_2 nanocomposite sample diluted 1:10 with distilled water using a Shimadzu UV–Vis spectrophotometer, and the spectrum was recorded in the spectrum mode. The recording wavelengths range from 200 to 800 nm.

2.2.2 Fourier transform infrared spectroscopy (FTIR)

FTIR was used to identify the functional groups in the synthesized CQDs/TiO_2 nanocomposite. The FTIR analysis was carried out using the potassium bromide (KBr) pelleting method, and this synthesized compound was mixed. The aqueous CQD samples were drop-casted onto KBr powder, ground, mixed, and pressed into a thin pellet. The sample was scanned at 500–4000 cm^{-1}.

2.2.3 X-ray diffraction (XRD)

X-ray diffraction (XRD) was used to determine the prepared samples' phase composition and crystal structure, with 2θ degrees ranging from 10° to 90°.

2.2.4 Scanning electron microscope (SEM)

The CQDs/TiO_2 Nanocomposites were further characterized using SEM to obtain structural details such as size and surface shape arrangement. SEM characterization was performed at IIT, BHU by using Nova Nano SEM.

2.2.5 Energy dispersive X-ray analysis (EDX)

EDX was used to analyze the types and quantity of elements at the present CQDs/TiO2 nanocomposite surface [14–17].

2.3 Measurement of photocatalytic activity

The photocatalytic activity of CQDs/TiO_2 Nanocomposites was studied by photodegrading a 10 ppm Methylene Blue solution in UV visible light (365 nm UV). The mixture was first stirred in the dark for 30 min to establish adsorption–desorption equilibrium before UV visible light irradiation.

Each sample was tested for 60 min using 0.1 g of photocatalyst and 50 mL of Methylene Blue solution. The first 30 min were spent in complete darkness, followed by 60 min of ultraviolet–visible light exposure. The samples were centrifuged at 6000 rpm for 30 min after photodegradation to separate the photocatalyst powder from the decolorized Methylene Blue (MB) solution. The solutions were then analyzed using a UV–visible spectrophotometer at 662 nm to obtain the relative concentration variation of the solutions [12, 18–20].

2.4 Molecular docking

Molecular docking studies were performed by maestro 12.9 module of Schrodinger software. Against SARS-COV-2 remdesivir used as FDA approved reference drug. Molecular docking steps are as follows.

2.4.1 Protein preparation

The first step in the molecular docking process is preparing the protein molecule. After importing the 3D structure of the SARS-COV-2 protein from PDB into Maestro 12.9, Protein Preparation Wizard (Prep Wizard) was used to prepare the protein. Prep Wizard performs several essential tasks, such as minimization, refining, and pre-processing. The PRIME correction was applied to the original PDB structure during preprocessing. Finally, the pre-processed protein structure was refined with restrained minimization using the OPLS_2005 force field.

2.4.2 Receptor grid generation

A grid was made precisely on the protein's binding site to make the molecular docking process easier. The active binding site of the co-crystallized ligand for proteins was surrounded by receptor grid boxes created by the "Glide's Receptor Grid Generation" module. The crystal structure was surrounded by a 20 Å radius for the receptor grid box and 10 Å × 10 Å × 10 Å for the computing cubic box.

2.4.3 Ligand preparation

Using Maestro 12.9's "import structure" file option, the drug molecules' 3D structures were acquired in SDF format to prepare them for molecular docking. The LigPrep wizard was then used to prepare the ligands and design the library. Using the OPLS_2005 force field and the energy function of small molecular mechanics with an RMSD cut-off of 10 Å, low-energy ligand isomers were obtained.

2.4.4 Molecular docking

A molecular docking study was carried out after the protein and ligand were prepared and the grid was created on the protein's active site. The binding energies were computed in Kcal/mol. Using the Glide Standard Precision (SP) protocol, a flexible docking approach was used without any constraints to predict the binding affinity and ligand efficiency, and their dock scores were reported [21–23].

2.5 CQD-TiO_2 nanocomposite computational modeling

2.5.1 CQD-TiO_2 structure modelling

The structure of citric acid carbon quantum dots was taken from the literature [24]. TiO_2 nanoparticles were modeled using the packing of the unit crystal cell taken from Cambridge Crystallographic Data Center, and the ID of the structure was 9015929 [25]. The packing was done along the a, b, and c axes, and a $4 \times 4 \times 2$ nano-particle with the formula $Ti_{253}O_{506}$ was obtained. Then, the modeling of CQD-$Ti_{253}O_{506}$ nanoparticle agglomerate was done using the MOPS algorithm, which is based on the use of the QM/MM technique and described in [Adsorption of Native Amino Acids on Nanocrystalline TiO_2: Physical Chemistry, QSPR, and Theoretical Modeling [26]. Briefly, in the MOPS method, there is an assumption that all structural changes occur during molecular motion (vibration, translation, and rotation) [26]. Adsorption of Native Amino Acids on Nanocrystalline TiO_2: Physical Chemistry, QSPR, and Theoretical Modeling [26]. Wilson's GF method is applied to find the directions of atomic motion, and the matrix equation is solved in the MOPS [27]. Some Mathematical Methods for the Study of Molecular Vibrations [27].

$$GFL = L\Lambda,$$

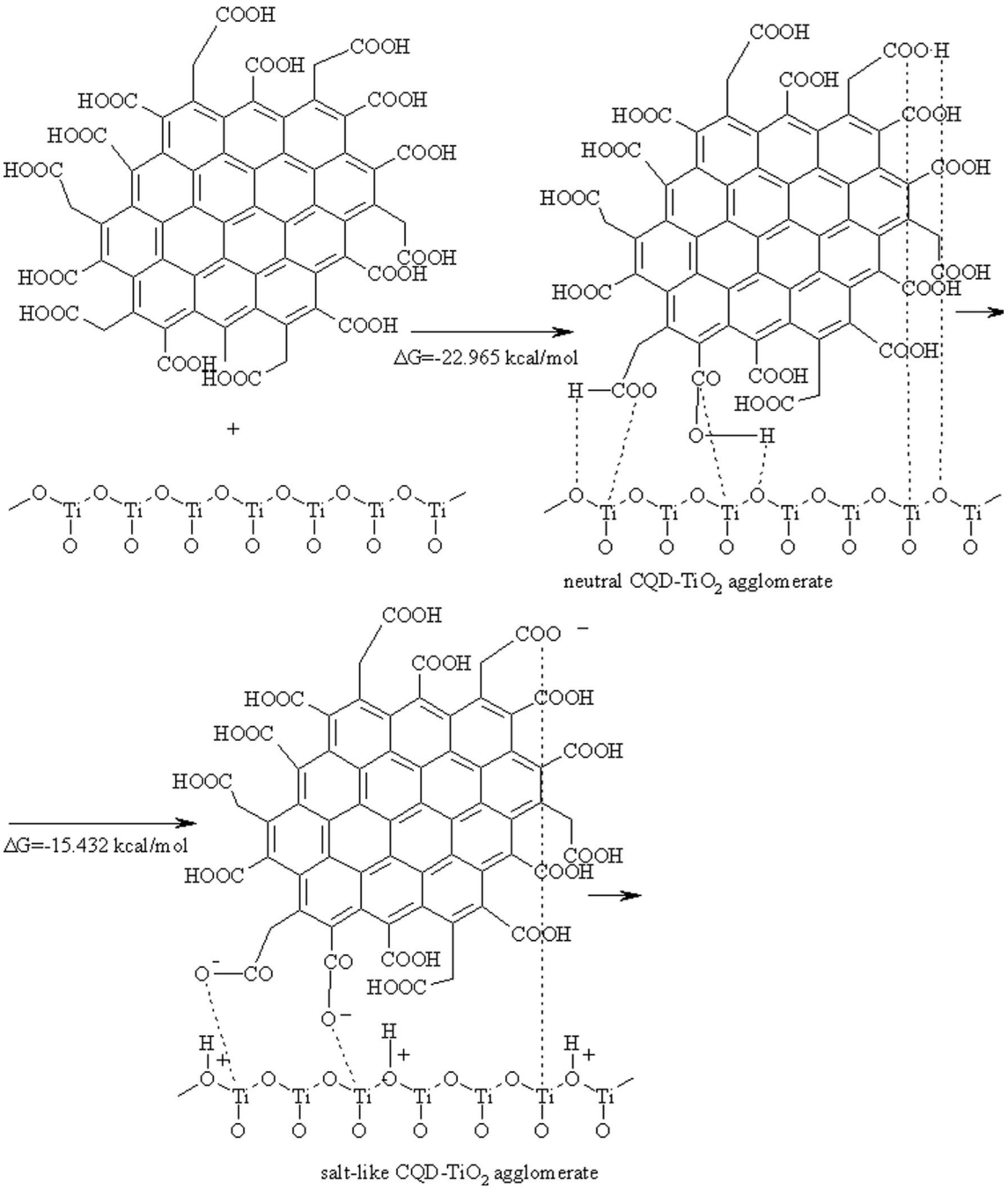

Scheme 1 Formation of the neutral and salt-like agglomerates and Gibbs free energies computed for each process

where F—matrix of force constants, the second derivatives of energy, G—inverse mass matrix, Λ, and L—eigenvalues and eigenvectors of the matrix A = GF. The elements of the diagonal Λ-matrix are the squares of vibrational, rotational, and translational frequencies. L-Vector shows the direction of atomic movements. MOPS searches for the agglomerate corresponding to the minimum potential energy.

The first modeling stage included determining the structures of the neutral agglomerate of CQD with a $Ti_{253}O_{506}$ nanoparticle. Next, the shortest contacts between the hydrogen atoms of the carboxyl groups of CQD and the oxygen atoms of $Ti_{253}O_{506}$ were determined. Since these interactions can lead to the migration of hydrogen atoms of carboxyl groups to the oxygen atoms of TiO_2, modeling of interactions of possible variants of the anionic form of CQD with the surface of titanium oxide containing newly formed OH groups (protonated $Ti_{253}O_{506}$) was carried out. As a result,

a second CQD-$Ti_{253}O_{506}$ nanoparticle agglomerates with a salt-like structure was obtained. Scheme 1 demonstrates the formation of the neutral and salt-like agglomerates and Gibbs free energies computed for each process.

2.5.2 Estimation of thermodynamic parameters

The Gibbs free energies of the processes of formation of 2 obtained agglomerates (the first one includes CQD and $Ti_{253}O_{506}$ nanoparticles in neutral forms, the second one is the salt-like CQD—$Ti_{253}O_{506}$ nanocomposite) were computed using the orbital-free quantum chemical method AlteQ, which uses approximation of electron density functions with Gaussians, as described in [28].

Gibbs free energies of the agglomerate formation were estimated using the following formula:

$$\Delta G = \Delta H - T\Delta S = H_{agglomerate} - H_{TiO2} - H_{CQD} - T(S_{agglomerate} - S_{TiO2} - S_{CQD})$$

where $H_{agglomerate}$, H_{TiO2}, H_{CQD} are enthalpies of formation and $S_{agglomerate}$, S_{TiO2}, S_{CQD} are entropies of the agglomerate, TiO_2 nanoparticle ($Ti_{253}O_{506}$), CQD, respectively.

In AlteQ, the enthalpy of formation is represented as follows:$H = c_{0(H)} + \sum_{A=1}^{N} c_{A(H)} N_A^{Sur}$

where $c_{0(H)}$ and $c_{A(H)}$ are parameters of the equation, $c_{A(H)}$ are parameters which depend on the position of the element of atom A in the Periodic Table, N is the number of atoms in the molecule, N_A^{Sur} is computed from overlap integrals [28].

Molecular entropy has been computed as follows:

$$S = c_{0(S)} + c_{1(S)} \sum_{A=1}^{N} N_A^{Sur}$$

where $c_{0(S)}$ and $c_{1(S)}$ are parameters of the equation.

2.5.3 Topological analysis of the electron density of the CQD-TiO_2nanoparticle

From the point of view of The Theory of Atoms in Molecules suggested by Richard Bader [29], the intermolecular contact between atoms belonging to different molecules of the agglomerate is characterized by the presence of (3,– 1) bond critical points of electron density in the intermolecular space of contacting molecules. To find these critical points, a topological analysis of the electron density of both CQD-$Ti_{253}O_{506}$ agglomerates was performed using the orbital-free quantum chemical method AlteQ, which recently showed promising results in the studies of large molecular systems [30].

3 Results and discussion

3.1 Synthesis of CQDs/TiO_2 nanocomposites

When citric acid is added to distilled water in a Teflon autoclave, heated over melting temperature, it decomposes and forms hydronium ions. These ions then function as catalysts in subsequent degradation reactions. A soluble polymer is formed when the carbon molecules undergo a polymerization reaction and condense. These soluble polymers undergo additional cycloaddition, promoting aromatic cluster formation. When these aromatcluster concentrations reach a critical supersaturation point, burst nucleation occurs, and CQDs are generated. After adding TiO_2 and CQD to a Teflon autoclave that was heated to melting temperature, condensation, cycloaddition, and condensation again, CQDs/TiO_2 nanocomposites were produced (Fig. 3).

3.2 Characterization of synthesized CQDs/TiO_2 nanocomposites

3.2.1 UV–vis absorption

UV spectra were recorded, and it attributes that the maximum absorbance of the final proposed compound CQDs/TiO_2 Nanocomposites was observed near 420 nm. It was regarding the carbon core & carbonyl functional groups on the surface of CQDs-TiO_2 Nanocomposites, which attributed to the π–π*, n–π* transition. The CQD under UV visible absorbance

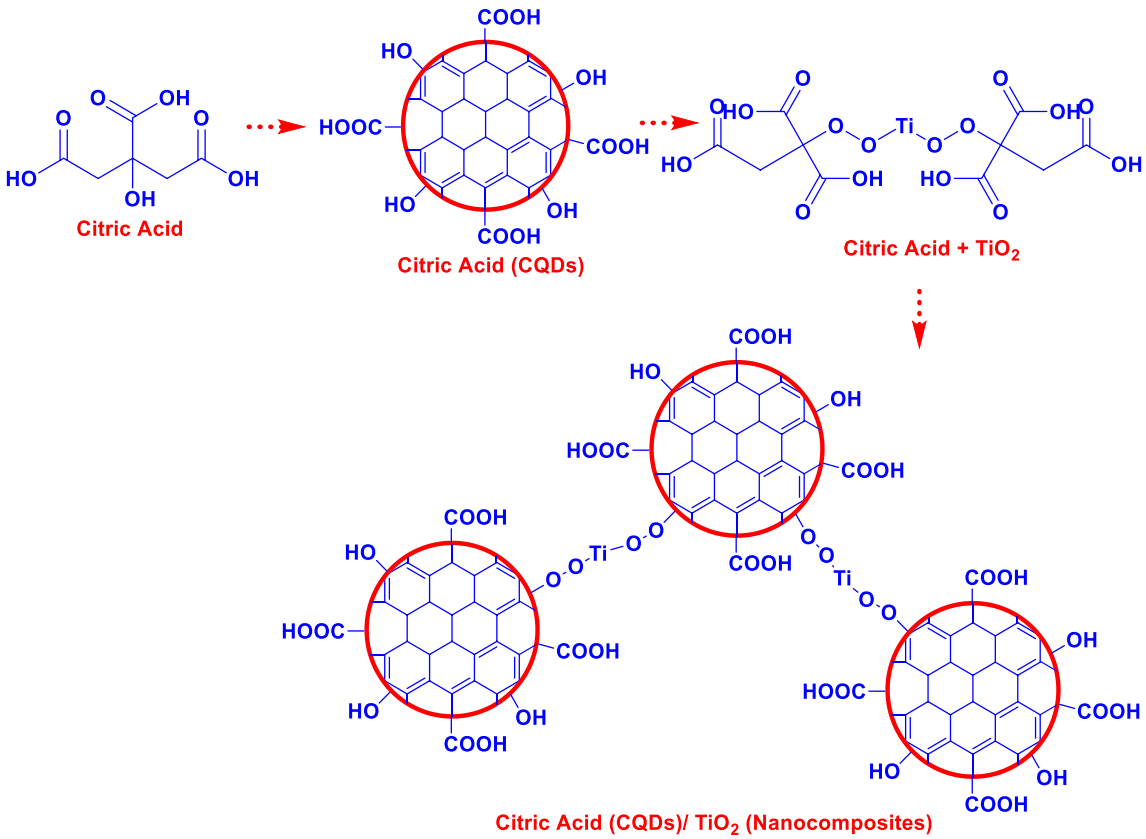

Fig. 3 Proposed Rxn involved in the synthesis of CQDs/TiO_2 Nanocomposites

is blue (Fig. 4a). The CQDs-TiO_2 Nanocomposites also showed the typical behavior of producing excitation-dependent fluorescence emission.

3.2.2 FTIR spectra

The nanocomposites of CQDs/TiO2 were characterized by FTIR spectroscopy, as observed in (Fig. 4b). The peak at 1505 cm^{-1} indicates the presence of sp^2 carbon. Other peaks observed include O–H stretching at 3164 cm^{-1} for carboxylic acid and Acyl C–O stretching at 1274 cm^{-1}. A spectral peak near 580 cm^{-1} Ti–O bond was observed.

3.2.3 XRD pattern of the CQDs/TiO_2 composite

In the X-ray diffraction pattern of nanocomposite ($n\lambda = 2d\sin\theta$) attributed to the presence of crystalline carbon ($d = 0.353$ nm, $d > 0.34$) calculated from Bragg's equation with highest intensity 8119 at angle 12.5781 (Fig. 4c).

3.2.4 SEM images of the CQDs/TiO_2 nanocomposites

The micrographs of the CQD-TiO_2 Nanocomposites (with size lower than 100 nm) were nearly spherical. The observation of lattice fringes indicated that the nanocomposites also had crystalline cores (Fig. 4d).

3.2.5 EDX analysis

EDX analysis of the CQDs/TiO_2 nanocomposite reveals the presence of Ti, C, and O, as shown in Fig. 4e. The narrow peaks at 0.3 and 0.8 keV represent C and O, respectively. The narrow peak at 4.4 keV is attributed to titanium.

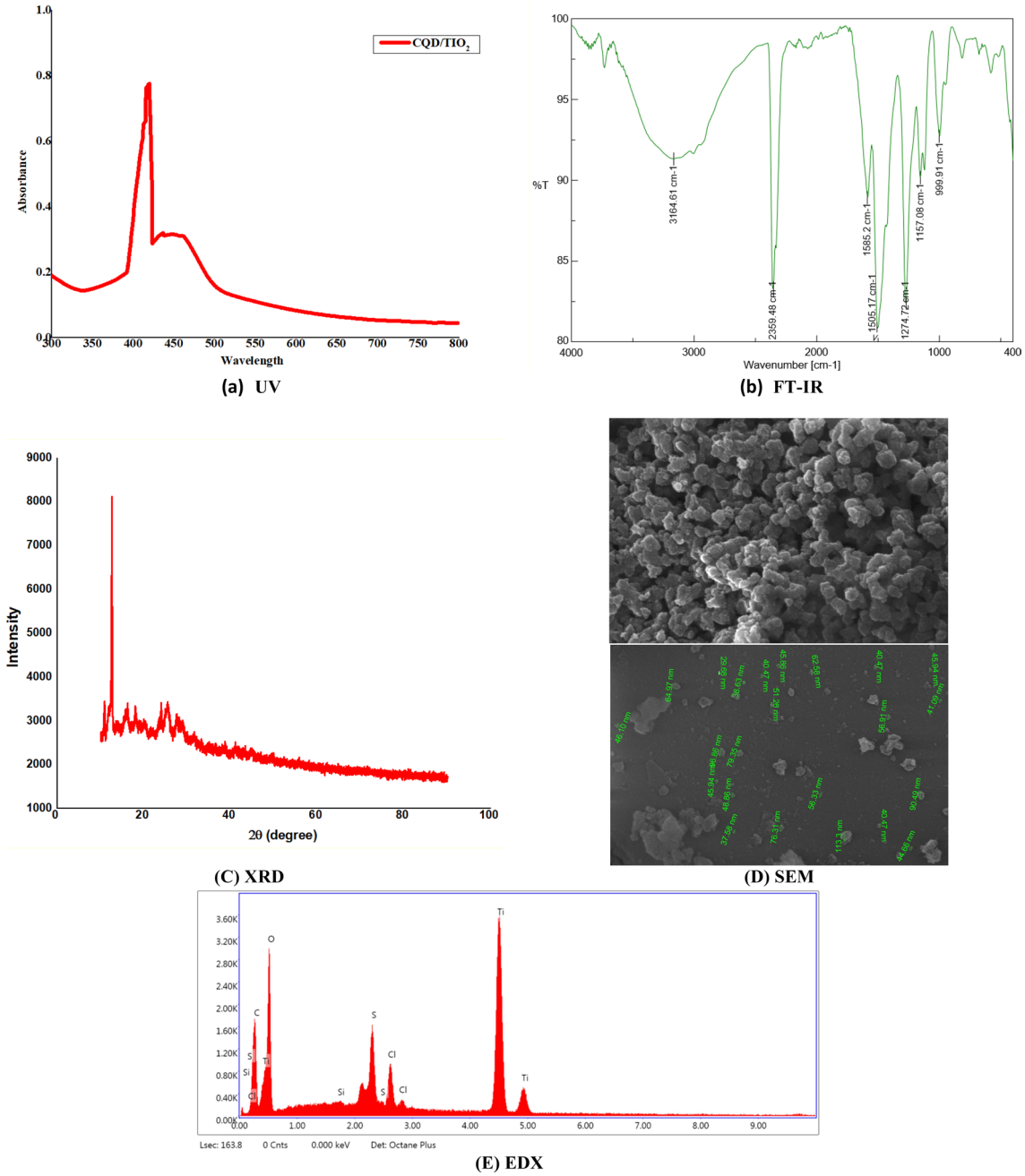

Fig. 4 Spectral characterization of synthesized Citric acid based CQDs/TiO_2 Nanocomposites

3.3 Photocatalytic performance analysis

The photocatalytic activity of citric acid, CQDs-citric acid, and CQDs/TiO_2 was determined by the photodegradation of Methylene Blue solution under UV visible light irradiation at 662 nm. Before the photocatalytic reaction, the aqueous suspension was stirred in the dark for 30 min to achieve adsorption/desorption equilibrium.

After 30 min of dark adsorption, citric acid, and CQDs/TiO_2 exhibited almost no MB adsorption. Figure 5 shows that, compared to citric acid, the MB concentration on citric acid CQDs/TiO_2 decreases more quickly. The degradation percentages of MB without photocatalyst, citric acid, CQDs-citric acid, and citric acid CQDs/TiO_2 nanocomposite were 5.68%, 84.23%, 96.23%, and 99.01%, respectively, with the same irradiation time of 60 min. Figure 5 compares the

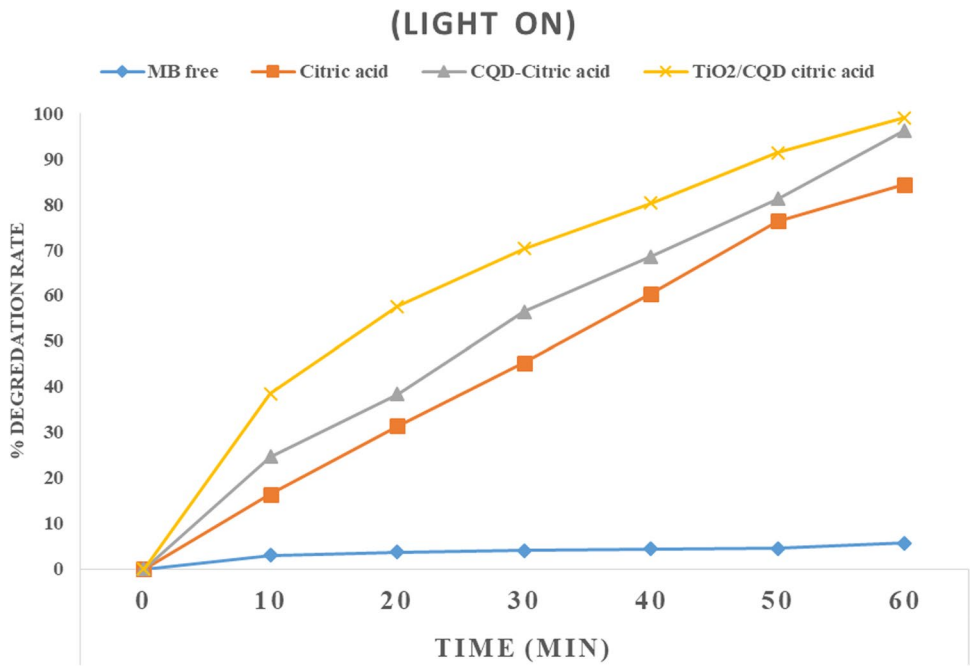

Fig. 5 Photocatalytic analysis of synthesized compounds

photocatalytic activity of citric acid, CQDs-citric acid, and CQDs/TiO_2 composites. CQDs/TiO_2 outperforms CQDs-citric acid, achieving a degradation ratio of ~ 99% after 60 min of ultraviolet irradiation.

3.4 Molecular docking studies

Citric acid and remdesivir as FDA approved drug were docked to the binding pocket of the SARS-COV-2 protein (PDB IDs: 7B3O), and the major binding interaction and 3D interaction diagram are reported in Table 1 and Fig. 6.

3.5 Computational study of the processes of formation of CQD-TiO_2 nano-composite

Modeling of the neutral form CQD-$Ti_{253}O_{506}$ agglomerate using MOPS showed that CQD is preliminarily adsorbed on the titanium dioxide surface with the formation of a series of three hydrogen bonds between the hydrogen atoms of the carboxyl group and the oxygen atoms of the titanium dioxide surface with a contact length of 2.08–2.29 Å (Fig. 7). Some hydrogen bonds are bifurcated, i.e. the hydrogen atom of the CQD simultaneously contacts the oxygen atoms of the titanium dioxide surface. Moreover, the carboxyl groups' oxygen atoms form contact with the surface's Ti atoms with a contact distance of 2.33–2.72 Å.

The presence of critical bond points confirms these intermolecular contacts. Table 2 shows the electron density values at each crucial point. The electron density values (ρ) show very effective interactions between CQD and titanium dioxide nanoparticles ($Ti_{253}O_{506}$); they vary in the 0.0662–0.1583 e/Å3 range.

In addition, there are forced interactions between the H (CQD) and Ti atoms as well as between O (CQD) and O ($Ti_{253}O_{506}$) atoms because these atoms are located close to oxygen and hydrogen atoms, forming hydrogen bonds. These contacts have ρ varying within 0.0358–0.0509 e/$Å^3$.

Table 1 Major Key interaction in molecular docking studies

Compound name	Docking score (Kcal/mol)	Hydrophobic interactions	H-bonding interactions
Citric acid	– 7.730	TYR365, ALA363, VAL362, CYS361, ILE358, VAL395, PHE392, CYS391	TYR365, CYS361, ASN360, THR393, PHE392,
Remdesivir	– 7.314	PHE486, TYR489, PHE490, LEU492, LEU91, TYR32, LEU33, VAL99, ALA100, ALA102	GLN 493, GLU484, ASP104

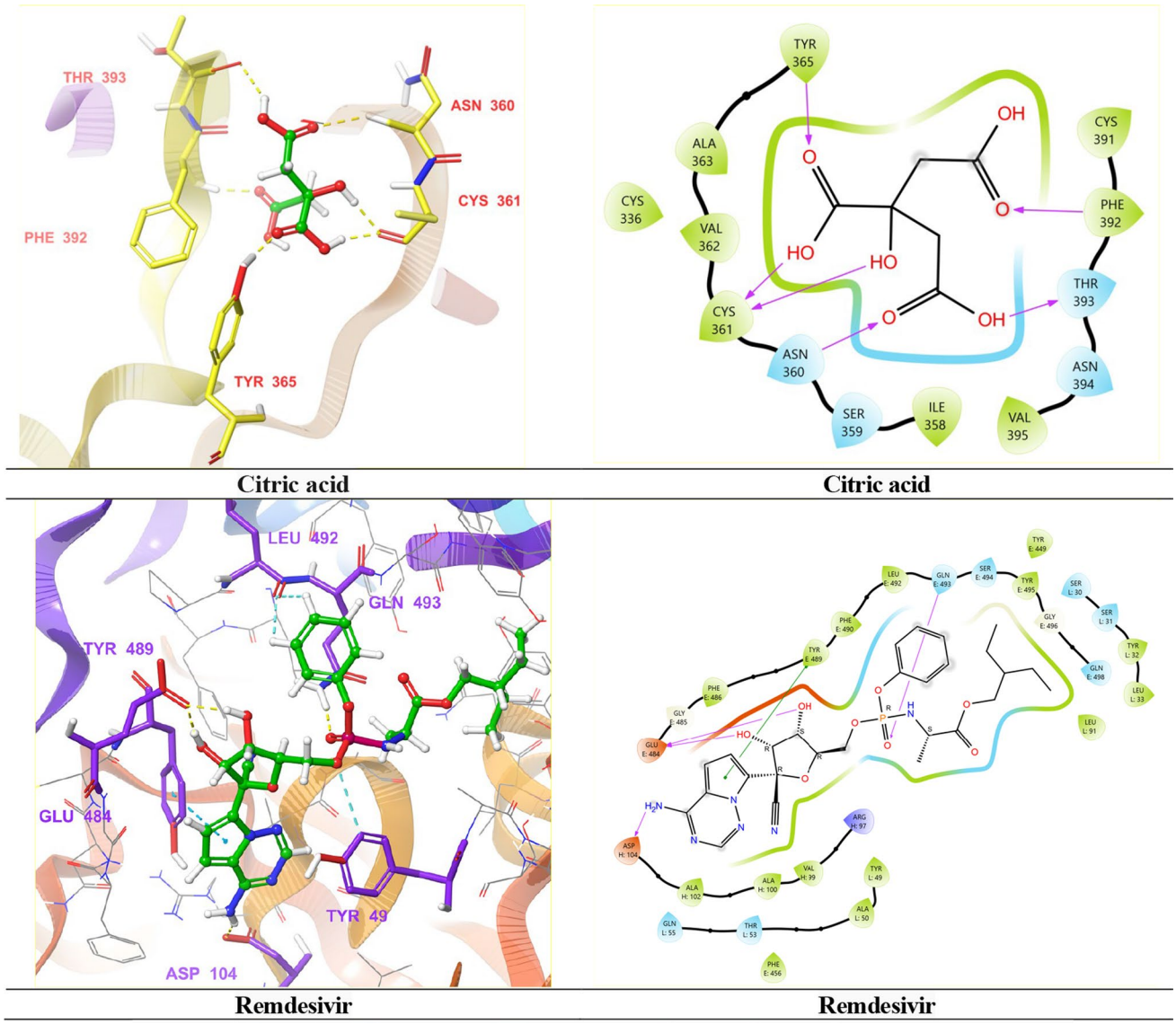

Fig. 6 2D & 3D-interaction diagram of Citric acid with SARS-COV-2 protein (PDB IDs: 7B3O)

The H(CQD) and O($Ti_{253}O_{506}$) interactions suggest the migration of CQD hydrogen atoms to titanium dioxide oxygen atoms and the formation of an anionic CQD structure with short contacts between the oxygen atom of carboxyl groups and Ti atoms. Thus, the CQD molecule we examined can simultaneously form 3 O-Ti bonds. To simulate the interactions of the proposed anionic form of CQD, the migration of hydrogen atoms to the nearest oxygen atoms of the surface of $Ti_{253}O_{506}$ was carried out (Scheme 1). The obtained salt-like agglomerate is shown in Fig. 8.

Figure 8 demonstrates effective O (anionic CQD)…Ti (protonated $Ti_{253}O_{506}$) contacts and O (anionic CQD)…H (protonated $Ti_{253}O_{506}$) hydrogen bonds. Electron density values at the (3,– 1) critical points for these salt-like interactions and hydrogen bonds vary in the range of 0.0328–0.1615 e/Å^3 (Table 3).

There are forced interactions: (1) between O (anionic CQD) and O (protonated $Ti_{253}O_{506}$) atoms; (2) between C (anionic CQD) and Ti (protonated $Ti_{253}O_{506}$) atoms; (3) between C (anionic CQD) and O (protonated $Ti_{253}O_{506}$) atoms. The contacts are formed because these atoms are located close to oxygen and hydrogen atoms, forming hydrogen bonds, and to oxygen and titanium atoms, forming salt-like bonds. These contacts are mostly less effective and have ρ varying within 0.0358–0.0509 e/Å^3.

An estimate of the Gibbs free energies using the AlteQ quantum chemical orbital-free method shows that both processes of formation of the neutral and salt-like agglomerates are beneficial (Scheme 1). The neutral CQD-$Ti_{253}O_{506}$ agglomerate is initially formed with a gain in Gibbs free energy of – 22.96 kcal/mol ($\Delta G = -22.965$ kcal/mol). Then,

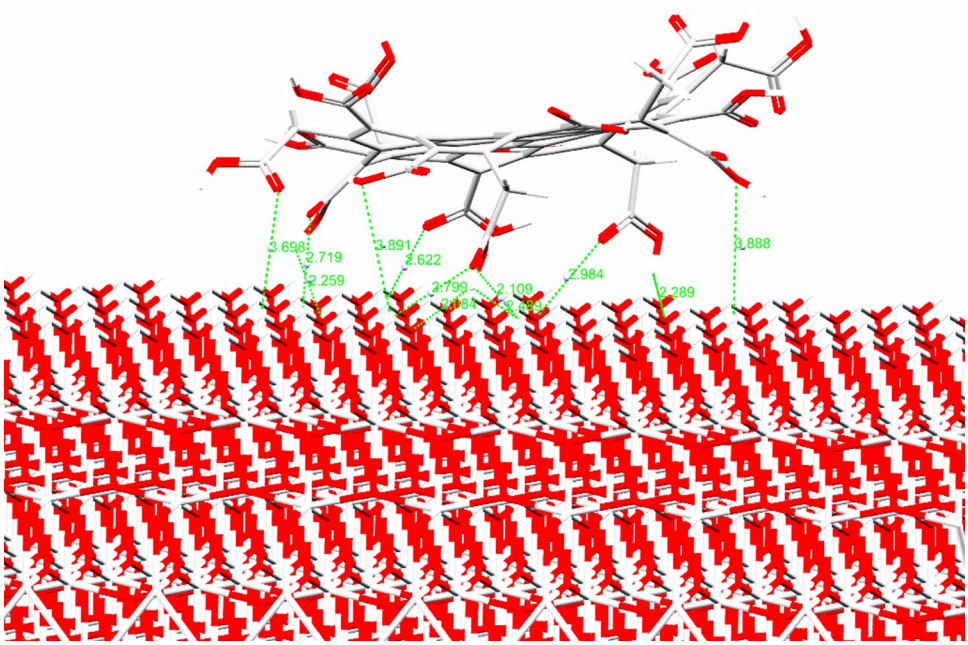

Fig. 7 Neutral CQD-$Ti_{253}O_{506}$ agglomerate. Blue points are (3,– 1) bond critical points of electron density. Green dotted lines show the most effective intermolecular contacts and their distances

Table 2 Electron density values (ρ) at the bond (3,–1) critical points between contacting atoms in the neutral CQD-$Ti_{253}O_{506}$ agglomerate

Atom of CQD	Atom of $Ti_{253}O_{506}$	ρ, e/Å^3
H	TI	0.0357762
O	TI	0.1413818
O	O	0.0435177
O	TI	0.0856157
H	O	0.0786439
O	TI	0.201064
H	O	0.1583378
H	O	0.1138414
O	TI	0.0662248
O	TI	0.0735933

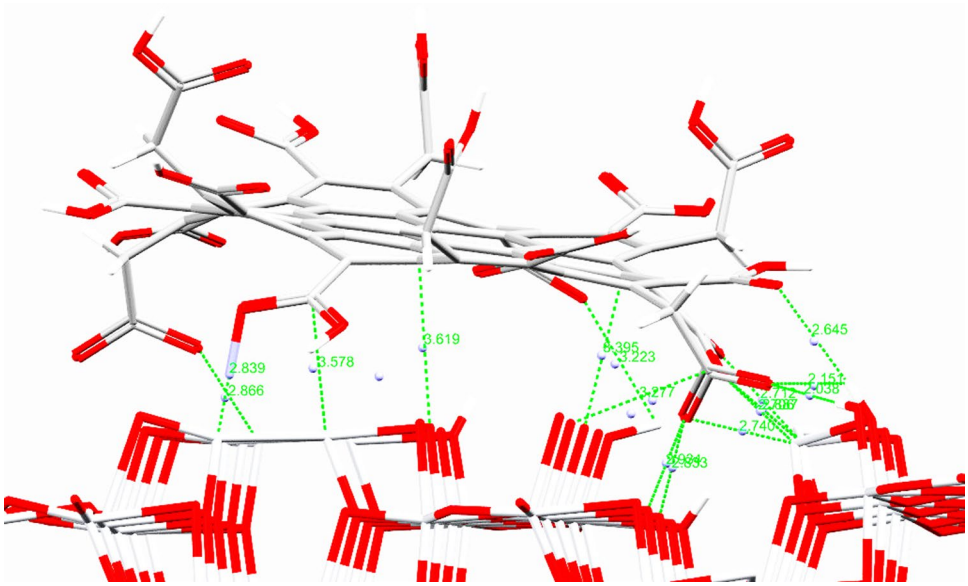

Fig. 8 Salt-like CQD-$Ti_{253}O_{506}$ agglomerate. Blue points are (3,– 1) bond critical points of electron density. Green dotted lines show the most effective intermolecular contacts and their distances

Table 3 Electron density values (ρ) at the bond (3,−1) critical points between contacting atoms in the salt-like CQD-$Ti_{253}O_{506}$ agglomerate

Anionic CQD	Protonated TiO_2	ρ, e/Å^3
O	TI	0.0607208
O	O	0.049743
C	TI	0.0263819
O	O	0.0394576
O	O	0.0306177
O	O	0.0503606
O	O	0.0145659
C	O	0.0209485
O	TI	0.0596722
O	TI	0.0740784
O	TI	0.0709658
O	H	0.1615836
O	H	0.0418423
O	TI	0.0583308
O	TI	0.0760492
O	H	0.1319792
O	TI	0.0327903

the migration of protons from the CQD to the titanium dioxide surface occurs with an additional gain in the Gibbs free energy of − 15.432 kcal/mol. The total increase in the Gibbs free energy of the processes is $\Delta G = -38.397$ kcal/mol. These processes are spontaneous from the point of view of thermodynamics.

3.6 Mechanism for photocatalytic degradation and charge carriers in CQDs/TiO_2

Based on the above results and discussion, Fig. 9 depicts a possible mechanism for the accelerated separation of charge carriers and enhanced photocatalytic activity of the CQDs/TiO_2 nanocomposites' visible-light-driven photodegradation process.

TiO_2 has gained much attention for its powerful photocatalytic antiviral action. Photogenerated holes on TiO_2 absorb oxygen from the air and convert it into active substances like ·OH, effectively removing pollutants. UV light exposure decomposes ambient oxygen and water, producing ROS such as •OH and $O_2-\bullet$ at the surface of TiO_2. These ROS can degrade the capsid/envelope proteins and phospholipids of non-enveloped/enveloped viruses, respectively. Furthermore, leakage and subsequent nucleic acid degradation cause viral particles to become inactivated over time. CQDs act as electron reservoirs, trapping photogenerated electrons from TiO_2's conduction band. This promotes the efficient separation of electrons and holes, thereby increasing photocatalytic activity. Furthermore, photogenerated electrons cause a transition from the visible to conduction bands. Further, the up-conversion property of CQDs allows long-wavelength light from visible light to be shifted to shorter wavelength light that TiO_2 can use.

Furthermore, under light conditions, CQDs may absorb photogenerated electrons from TiO_2 and react with oxygen on its surface to produce oxygen-free radicals, further degrading the dye and achieving photocatalytic activity. Hojkova et al., reported a multifunctional photocatalytic effect of TiO_2 thin films, including photodegradation with antiviral properties. Furthermore, modified TiO_2 has proven to be very useful in visible light activity applications for both indoor and outdoor environments. This photocatalytic disinfection effect has also been shown to be very promising in controlling various viruses as an antiviral photocatalyst. Thus, illumination of TiO_2 photocatalyst generates highly reducing/oxidizing free radicals that have excellent antiviral activity against a variety of viruses, including influenza virus, which is transmitted via aerosol and causes respiratory tract infection similar to COVID-19. Khaibullina et al., reported that a photoresposive coating based on TiO_2 NPs exposed to UV light was effective in deterring the proliferation of COVID-19 surrogates and destroying viral particles. The preceding discussion demonstrates that TiO_2-based photocatalyst nanomaterials are extremely promising for antiviral activity. The antiviral efficacy of CQDs/TiO_2 against SARS-CoV-2 has yet to be thoroughly investigated [20, 31–33].

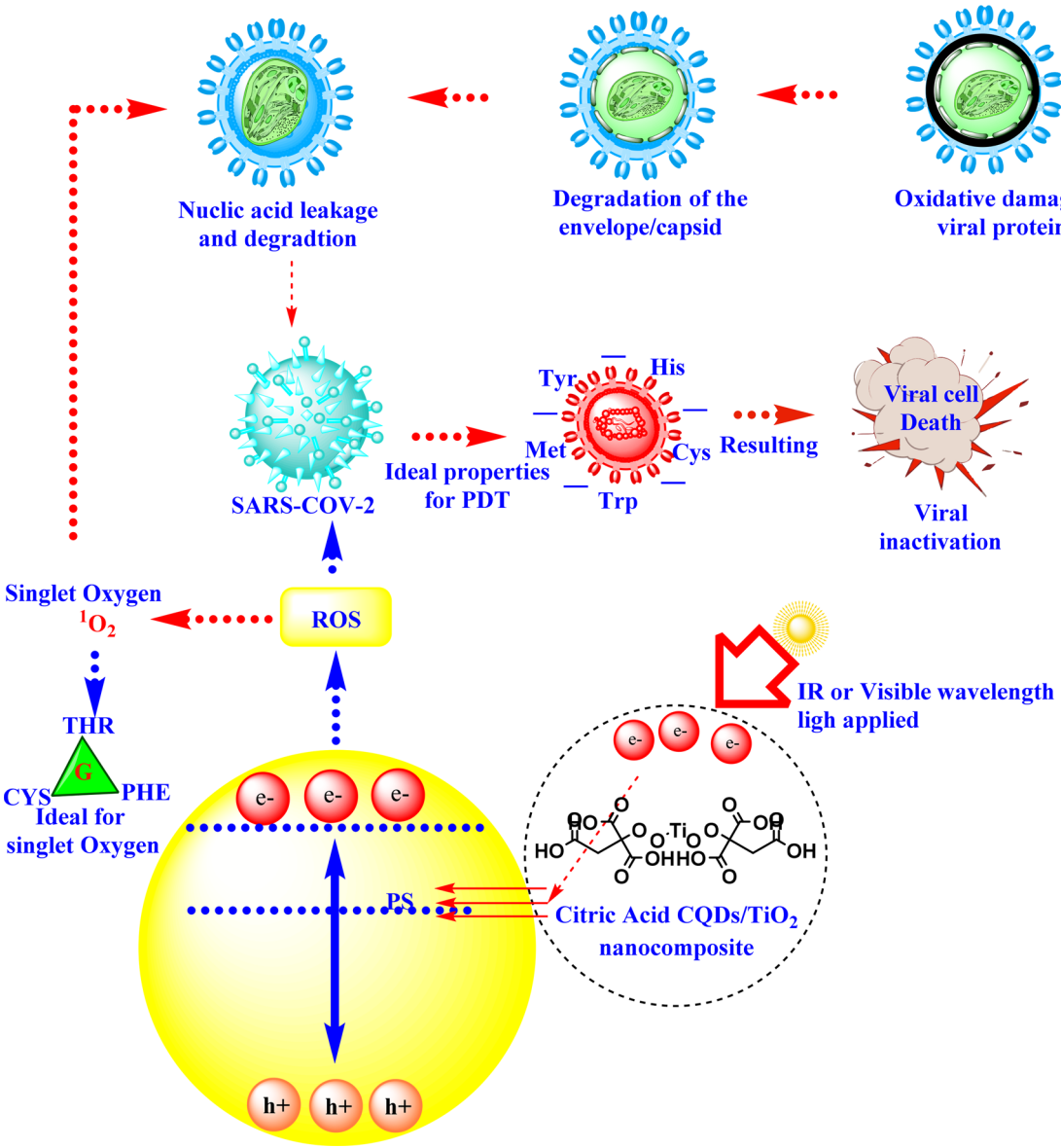

Fig. 9 Mechanism for Photocatalytic degradation & charge carriers in CQDs/TiO_2

4 Conclusion

The synthesis of citric acid carbon quantum dots and their composites with titanium dioxide were done by hydrothermal method with the use of teflon coated stainless steel autoclave and thermal method at different pH, temperature, and time and selected best-optimized method—UV, IR, SEM, EDX, XRD, etc., characterized all nanocomposites. Photocatalysis activity of synthesized CQDs/TiO_2 nanocomposites and quantum dots has been done under long UV, and their mechanism is understood. Computational modeling and AlteQ quantum chemical computations of the agglomerates of CQD and titanium dioxide nanoparticles with the composition $Ti_{253}O_{506}$ showed 2 stages of nanocomposite formation. One of them is the formation of the neutral form of CQD-$Ti_{253}O_{506}$ agglomerate. The second one is the salt-like CQD-$Ti_{253}O_{506}$ agglomerate obtained after the migration of protons of COOH groups of CQD to the titanium dioxide surface. The total gain in the Gibbs free energy of the processes was − 38.397 kcal/mol, corresponding to intermolecular solid interactions comparable in energy to the energies of covalent bonds. *In-silico* screening was done using Schrodinger software, and molecular docking of citric acid was done against the SARS-COV-2 protein. Molecular docking studies of citric acid showed good binding interaction with SARS-COV-2 protein. The photocatalytic activity of CQDs/TiO_2 showed extremely

promising results. Based on this study, the proposed mechanism of action of these compounds is reported in this manuscript. A detailed investigation of CQDs/TiO_2 against SARS-CoV-2 is needed, which is another part of the research in our next manuscript. The nanoscale size of the CQDs/TiO_2 PDT agent ensures precise localization of the potential drug at the site of the action. We hypothesize that this will exert a multi-prolonged action against SARS-COV-2 without toxicity. Future research expects to seek CQDs with unique optical properties and involve many applications such as different bio-applications (biosensing and bioimaging).

Acknowledgements The authors thank the Science & Engineering Research Board (SERB) in New Delhi, India for the financial support of ASEAN-India collaborative research project grant number (CRD/2021/000433). They are also thankful to Sam Higginbottom University of Agriculture, Technology & Sciences (SHUATS) in Prayagraj, India, Universiti Sains Malaysia (USM) in Malaysia, and Ubon Ratchathani University (UBU) in Thailand. The part of the work of Maria Grishina and Nadezhda Palko were carried out with the support of the Ministry of Science and Higher Education of the Russian Federation on the basis of the Federal State Autonomous Educational Institution of Higher Education "SUSU (National Research University)" (agreement No. 075-15-2022-1135 dated 07/01/2022).

Author contributions Conceptualization: Amita Verma, Hooi Ling Lee, Purim Jarujamrus, and Maria Grishina; Data collection: Ankit Kumar Singh, Nurul Hidayah Mohamad Idris, Nattasa Kitchawengkul, Nadezhda Palko; Writing the manuscript: Ankit Kumar Singh, Joina Gunjan Singh, Nadezhda Palko; Sketching of Figures and data interpretation: Ankit Kumar Singh, Nadezhda Palko; Writing, review and final editing of the manuscript: Amita Verma, Hooi Ling Lee, Purim Jarujamrus, Maria Grishina and Prateek Pathak.

Funding NA.

Data availability The data that support the findings of this study is original research based.

Code availability NA.

Declarations

Competing interests The authors declare no competing interests.

References

1. Malavika JP, Shobana C, Sundarraj S, Ganeshbabu M, Kumar P, Selvan RK. Green synthesis of multifunctional carbon quantum dots: an approach in cancer theranostics. Biomater Adv. 2022;136: 212756.
2. Yadav H, Rout D, Upadhyaya AK, Agarwala P, Sharma A, Sasmal DK. Carbon quantum dots for efficient delivery of curcumin in live cell. Chem Phys Impact. 2023;7: 100279.
3. Choi D, Ham S, Jang D-J. Visible-light photocatalytic reduction of Cr (VI) via carbon quantum dots-decorated TiO2 nanocomposites. J Environ Chem Eng. 2018;6(1):1–8.
4. Kipshidze N, Yeo N, Kipshidze N. Photodynamic and sonodynamic therapy of acute hypoxemic respiratory failure in patients with COVID-19. Photodiagn Photodyn Ther. 2020;31: 101961.
5. Łoczechin A, Séron K, Barras A, Giovanelli E, Belouzard S, Chen Y-T, Metzler-Nolte N, Boukherroub R, Dubuisson J, Szunerits S. Functional carbon quantum dots as medical countermeasures to human coronavirus. ACS Appl Mater Inter. 2019;11(46):42964–74.
6. Zhang L-Y, Han Y-L, Yang J-J, Deng S-L, Wang B-Y. Construction and photocatalysis of carbon quantum dots/layered mesoporous titanium dioxide (CQDs/LM-TiO2) composites. Appl Surf Sci. 2021;546: 149089.
7. Xue Y, Liu C, Andrews G, Wang J, Ge Y. Recent advances in carbon quantum dots for virus detection, as well as inhibition and treatment of viral infection. Nano Converg. 2022;9(1):15.
8. Sargin I, Yanalak G, Arslan G, Patir IH. Green synthesized carbon quantum dots as TiO2 sensitizers for photocatalytic hydrogen evolution. Int J Hydrogen Energy. 2019;44(39):21781–9.
9. Mahmoudi H: Photodynamic therapy as a new technology for inactivation of coronavirus disease (covid-19). Fron Biomed Technol. 2022.
10. Tariq R, Khalid UA, Kanwal S, Adnan F, Qasim M. Photodynamic therapy: a rational approach toward COVID-19 management. J Exp Res Pharmacol. 2021;6(2):44–52.
11. Svyatchenko VA, Nikonov SD, Mayorov AP, Gelfond ML, Loktev VB. Antiviral photodynamic therapy: inactivation and inhibition of SARS-CoV-2 in vitro using methylene blue and Radachlorin. Photodiagn Photodyn Ther. 2021;33: 102112.

12. Shen T, Wang Q, Guo Z, Kuang J, Cao W. Hydrothermal synthesis of carbon quantum dots using different precursors and their combination with TiO2 for enhanced photocatalytic activity. Ceram Int. 2018;44(10):11828–34.
13. Lu Y, Guan S, Hao L, Yoshida H, Nakada S, Takisawa T, Itoi T. Inactivation of SARS-CoV-2 and photocatalytic degradation by TiO2 photocatalyst coatings. Sci Rep. 2022;12(1):16038.
14. Janus Ł, Radwan-Pragłowska J, Piątkowski M, Bogdał D. Coumarin-modified CQDs for biomedical applications—two-step synthesis and characterization. Int J Mol Sci. 2020;21(21):8073.
15. Singh I, Arora R, Dhiman H, Pahwa R. Carbon quantum dots: synthesis, characterization and biomedical applications. Turk J Pharm Sci. 2018;15(2):219–30.
16. Saraswat SK, Mustafa MA, Ghadir GK, Kaur M, Lozada DFG, Al-Ani AM, Alshahrani MY, Abid MK, Jumaa SS, Alhameedi DY. Carbon quantum dots: a comprehensive review of green Synthesis, characterization and investigation their applications in bioimaging. Inorganic Chem Commun. 2024:112279.
17. Patel V, Shah J, Gupta AK. Design and In-silico study of bioimaging fluorescence Graphene quantum dot-Bovine serum albumin complex synthesized by diimide-activated amidation. Comput Bio Chem. 2021;93: 107543.
18. Ayad MM, Elmorsy E, Amer WA, Mahrous A. Insight into the novel Zif-8@ N-Cqds/Zif-67 nanocomposite for photocatalytic degradation of methylene blue under visible light irradiation. Zif-67 Nanocomposite for Photocatalytic Degradation of Methylene Blue Under Visible Light Irradiation.
19. Williams IBI, Kouadio Fodjo E, Amadou K, Albert T, Kong C. Enhancing the photocatalytic activity of TiO2 nanoparticles using green carbon quantum dots. Int J Nano Dimens. 2022;13(2):144–54.
20. Hidayat RN, Widiyandari H, Parasdila H, Prilita O, Astuti Y, Mufti N, Ogi T. Green synthesis of ZnO photocatalyst composited carbon quantum dots (CQDs) from lime (Citrus aurantifolia). Catalysis Comm. 2024:106888.
21. Pauly I, Kumar Singh A, Kumar A, Singh Y, Thareja S, Kamal MA, Verma A, Kumar P. Current insights and molecular docking studies of the drugs under clinical trial as RdRp inhibitors in COVID-19 treatment. Curr Pharma Design. 2022;28(46):3677–705.
22. Singh AK, Sreelakshmi P, Pathak P, Kumar A, Singh H, Yadav JP, Verma A, Grishina M, Kumar P. Design, virtual screening, molecular docking, ADME and cytotoxicity studies of 1, 3, 5-triazine containing heterocyclic scaffolds as selective BRAF monomeric, homo and heterodimeric inhibitors. Comb Chem High Throughput Screening. 2024.
23. Singh AK, Kumar A, Arora S, Kumar R, Verma A, Khalilullah H, Jaremko M, Emwas AH, Kumar P. Current insights and molecular docking studies of HIV-1 reverse transcriptase inhibitors. Chem Biol Drug Des. 2024;103(1): e14372.
24. Dong Y, Shao J, Chen C, Li H, Wang R, Chi Y, Lin X, Chen G. Blue luminescent graphene quantum dots and graphene oxide prepared by tuning the carbonization degree of citric acid. Carbon. 2012;50(12):4738–43.
25. Howard C, Sabine T, Dickson F. Structural and thermal parameters for rutile and anatase. Acta Crystallogr Sect B Struct Sci. 1991;47(4):462–8.
26. Shchelokov A, Palko N, Potemkin V, Grishina M, Morozov R, Korina E, Uchaev D, Krivtsov I. Bol'shakov O: Adsorption of native amino acids on nanocrystalline TiO2: physical chemistry, QSPR, and theoretical modeling. Langmuir. 2018;35(2):538–50.
27. Wilson EB Jr. Some mathematical methods for the study of molecular vibrations. J Chem Phys. 1941;9(1):76–84.
28. Potemkin V, Grishina M. Electron-based descriptors in the study of physicochemical properties of compounds. Comput Theor Chem. 2018;1123:1–10.
29. Bader RF, Molecules AI. A quantum theory. Oxford, UK: Clarendon; 1990.
30. Grishina MA, Potemkin VA. Topological analysis of electron density in large biomolecular systems. Curr Drug Dis Technol. 2019;16(4):437–48.
31. Markowska-Szczupak A, Paszkiewicz O, Yoshiiri K, Wang K, Kowalska E. Can photocatalysis help in the fight against COVID-19 pandemic? Curr Opin Green Sust Chem. 2023;40: 100769.
32. Shafique M, Mahr MS, Yaseen M, Bhatti HN. CQD/TiO2 nanocomposite photocatalyst for efficient visible light-driven purification of wastewater containing methyl orange dye. Mater Chem Phys. 2022;278: 125583.
33. Prakash J, Cho J, Mishra YK. Photocatalytic TiO2 nanomaterials as potential antimicrobial and antiviral agents: scope against blocking the SARS-COV-2 spread. Micro Nano Eng. 2022;14: 100100.